coatings

MDPI

Article

Static and Dynamic Magnetic Properties of FeGa/FeNi (FeNi/FeGa) Bilayer Structures

Zhen Wang [1,2], Fenglong Wang [1], Zhaoyang Hou [1], Chunlong Xu [1] and Derang Cao [3,*]

1 Department of Applied Physics, Chang'an University, Xi'an 710064, China; wangzhen@chd.edu.cn (Z.W.); wangfenglong@chd.edu.cn (F.W.); houzy@chd.edu.cn (Z.H.); chunlongxu@chd.edu.cn (C.X.)
2 Center for Spintronics and Quantum Systems, State Key Laboratory for Mechanical Behavior of Materials, Xi'an Jiaotong University, Xi'an 710049, China
3 College of Physics, National Demonstration Center for Experimental Applied Physics Education, Qingdao University, Qingdao 266071, China
* Correspondence: caodr@qdu.edu.cn

Received: 9 March 2020; Accepted: 6 April 2020; Published: 14 April 2020

Abstract: FeGa/FeNi bilayer structures with different deposition order were fabricated by the electrodeposition method on indium tin oxide (ITO) substrates. The structure, morphology, static and dynamic magnetic properties of FeGa/FeNi (FeNi/FeGa) films were investigated. The bilayer structures exhibit extremely various magnetic properties with different deposition order which could be attributed to the different coupling interaction in the interface. When FeGa is on top, the bilayer structures show lower coercivity than when FeNi is on top. Meanwhile, increase of the proportion of FeNi in the bilayer structure could affect the H_c and M_r/M_s. The ferromagnetic resonance peak of FeGa on top moves to a high field compared with FeNi on top. Moreover, FeGa on top shows improved complex permeability and a clear resonant phenomenon of the magnetization. These properties make FeGa/FeNi bilayer structure a potential candidate for high-frequency application.

Keywords: FeGa/FeNi bilayer structure; electrodeposition; coercivity; ferromagnetic resonance; permeability

1. Introduction

As a fascinating magnetostrictive material, iron-gallium (FeGa) alloy has been widely investigated due to its good mechanical properties with maximum magnetostriction of 350 ppm under a low magnetic field when the content of Ga is 19% [1–4]. FeGa also exhibits excellent soft magnetic properties and metallic ductility, which make it a fantastic potential candidate in fabricating more efficient, faster, and smaller high-frequency devices for the applications of including recording heads, wireless inductors, and microwave noise filters [5–7]. Recently, FeGa film deposited on a flexible substrate was proposed [8,9]. The results show that the clamping effect of the sample deposited on stiff substrates is reduced and meanwhile the anisotropy of the magnetostrictive film improved. In addition, the magnetic properties and magnetostriction of FeGa films also can be tuned through the stress induced by a flexible substrate [10].

Otherwise, FeGa materials can be used to optimize the static and dynamic magnetic properties of the sample. In particular, the soft magnetic properties of FeGaNi film and FeGa/FeNi multilayer films improve due to the introduced FeGa species [11,12]. Giant magnetoimpedance effect of $Fe_{75.5}Cu_1Nb_3Si_{13.5}B_7$ amorphous ribbon can be obviously enhanced by covering FeGa film on the surface of the sample [13]. It has been demonstrated that changing the film's shape, doping, and interface of heterostructures with different layers and thicknesses can improve the coercivity and anisotropy field which promotes the high-frequency magnetic applications requiring strong magnetoelastic coupling [14–16].

Various heterostructures show different synergistic relations between two or more building blocks that improve the functional characteristics [17,18]. The remanent magnetization and the exchange bias of FeGa/IrMn heterostructures could be remarkably changed by means of improving the strength and the orientation of the uniaxial magnetic anisotropy [19]. For the heterostructure of hard and soft ferromagnets in thin film, strong exchange spring magnetism is benefited to improve static and dynamic magnetic properties. The coupling between the hard and soft ferromagnetic layers can effectively reduce the energy required to flip the moment of the film [20,21]. Some excellent works have involved the magnetoelastic and high-frequency properties of FeGa/magnetic heterostructures or multilayers, such as FeGa/FeNi and FeGa/Mn heterostructures [11,22]. The results show low coercivity, high permeability, and high strain sensitivity properties which make them extremely promising applications in high-frequency, strain coupled multiferroic systems.

In this work, we fabricated FeGa/FeNi bilayer heterostructures on indium tin oxide (ITO) by the electrodeposition method. The electrodeposition method is easy to implement when compared with sputtering. The method more easily generates defects or various morphologies with different reactive and additive materials. Different interface coupling interactions between the layers could be introduced by the deposition sequences, and this will make the films present various magnetic properties. Thus, we fabricated FeGa/FeNi bilayer heterostructures with different deposition order to tune the static and dynamic magnetic properties of FeGa/FeNi heterostructures.

2. Materials and Methods

2.1. Preparation

All the electrochemical experiments were performed at room temperature using an electrochemical workstation (CHI 860D) with a conventional three electrode configuration. The reference electrode was the saturated calomel electrode and a platinum (Pt) strip with an area of 4 cm^2 was used as counter electrode. The working electrode was ITO conductive glass. For the FeNi layer, the electrolyte was in a single mixed solution composed of $FeSO_4 \cdot 7H_2O$ (0.05 mol/L, Beijing Chemical Reagent Company, Beijing, China), $NiSO_4 \cdot 7H_2O$ (0.05 mol/L, Fengshun Fine Chemicals Company, Shanghai, China) combined with boric acid (0.5 mol/L, Beijing Chemical Reagent Company, Beijing, China) as a pH buffer, ascorbic acid (1 g/L, Beijing Chemical Reagent Company), glycine (2 g/L, Beijing Chemical Reagent Company, Beijing, China) and saccharine (2 g/L, Beijing Chemical Reagent Company) as complexing agents to keep the ferrous iron and nickel from oxidizing. For the FeGa layer, the contents of electrolytes were composed of $FeSO_4 \cdot 7H_2O$ (0.04 mol/L), $Ga_2(SO_4)_3 \cdot 16H_2O$ (0.05 mol/L, Alfa Aesar Company, Tewksbury, MA, USA), boric acids (30 g/L), ascorbic acids (5 g/L), and sodium citrate (25 g/L, Beijing Chemical Reagent Company, Beijing, China). The pH of the solution was adjusted to 4.8 by NaOH (Tianhe Chemical Reagent Factory, Tianjin, China). All deposition potential was −1.3 V and all chemicals were reagent grade and solved in distilled water. The experiments kept every solution concentration unchanged so that we could regulate the electrodeposition time in order to obtain the films with different thicknesses. Thus, different thicknesses of FeGa and FeNi were deposited in the top or bottom layer with different deposition times, as shown in Table 1.

Table 1. Sample name with deposition condition.

Bottom layer	FeGa (500 s)	FeNi (200 s)	FeGa (200 s)	FeNi (500 s)	FeGa (500 s)	FeNi (500 s)
Top layer	FeNi (200 s)	FeGa (500 s)	FeNi (500 s)	FeGa (200 s)	FeNi (500 s)	FeGa (500 s)
Name	SA1	SA2	SB1	SB2	SC1	SC2

2.2. Characterization

The crystal structure was analyzed by X-ray diffraction (XRD, PANalytical X'Pert) with Cu-Ka radiation (λ = 1.5406 Å). Film thicknesses were determined with a surface profile meter (Dektak 8).

A field emission scanning electron microscope (FESEM, Hitachi S-4800, Tokyo, Japan) was utilized to investigate the surface topography of the samples. Meanwhile, the elemental compositions of the films were carried out by an energy-dispersive X-ray spectrometer (EDX, Hitachi S-4800, Tokyo, Japan). The hysteresis loops for samples with various curving degrees were measured by vibrating sample magnetometer (VSM, Lakeshore 7304, Columbus, OH, USA) at room temperature, and the magnetic field was applied parallel to the film plane. The ferromagnetic resonance measurements were performed by using an X-band spectrometer (f = 9 GHz, JEOL, JESFA300, München, Germany) at room temperature. The permeability spectra were obtained in zero bias field by using a vector network analyzer (Agilent E8363B, Santa Clara, CA, USA) with a shorted microstrip transmission-line perturbation method.

3. Results and Discussion

3.1. Structure and Morphology of FeNi/FeGa(FeGa/FeNi) Bilayer

3.1.1. Structure

XRD patterns of all FeGa/FeNi (FeNi/FeGa) bilayer structures are displayed in Figure 1. As shown clearly, it is noticed that all the samples show a polycrystalline structure and the strength of the peaks is weak which means the structures have a large amorphism. The diffraction peak at 35.4 degrees comes from the ITO (222) substrate. The peaks at 44.6, 60, and 82 degrees are corresponding to (110), (200), and (211) of FeNi or FeGa, respectively. The strength of the peaks indicates that the polycrystalline alloys show the growth direction is along a slightly preferred orientation (110). However, these diffraction peaks are hard to help us to tell the difference between FeNi and FeGa from the patterns, because their peaks are in the similar positions. Thus, the compositions of the films were determined by an EDX. The mean atomic ratio of Fe/Ga was about 82/18 and Fe/Ni was about 65/35 with this preparation method. Through the surface profile meter, the thickness of FeNi was about 196 and 371 nm for deposition time 200 and 500 s from the reference samples, respectively. Meanwhile, the thickness of FeGa was about 82 and 234 nm for 200 and 500 s, respectively.

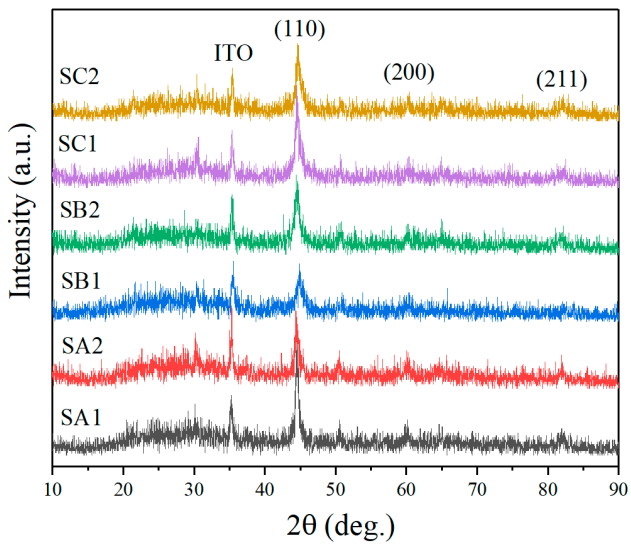

Figure 1. X-ray diffraction (XRD) spectra for SA1, SA2, SB1, SB2, SC1, and SC2.

3.1.2. Morphology

The morphology of the samples is characterized by SEM in Figure 2. One can see that the surface of SA1, SB1, and SC1 exhibits as granular for FeNi on the top of the FeGa layer (Figure 2a,c,e) and the average diameter is about 221.6, 240.7, and 304.5 nm, respectively. The diameter of SB1 or SC1 is

larger than that of SA1 which may come from the longer deposition time for the FeNi layer in SB1 and SC2, but the difference in diameter for SB1 and SC1 may be caused by the error of concentration ratio of the solution in the experiment. In Figure 2b,d,f, when FeGa is on the top, the surfaces show a rice-like granular appearance for SA2, SB2, and SC2 and the rice-like particles show almost the same mean length and width at about 180 and 80 nm. The insets show the cross-section of the sample. The thicknesses of the films are 453.8, 461.5, 445.2, 459.7, 584.3, and 607.8 nm for SA1, SA2, SB1, SB2, SC1, and SC2, respectively, which roughly correspond to the surface profile meter results. Meanwhile, a similar columnar structure with columns perpendicular to the film plane for the samples can be found, but the boundary of these columnar structures in each cross-sectional image are hard to distinguish clearly. The dividing line between the ITO substrate and the bilayer structure is visible and is indicated in the images. Moreover, from the insets of Figure 2d,f, there seems to be a dividing line at about 230 nm above ITO and the size of columnar structures seems a little different on up and down sides of the boundary. For other bilayer films, the boundary between FeNi and FeGa layers is not clear. Generally, the coupling interaction between bilayers would be affected by the morphology in the interface. In the SEM images, we find that the morphology is very different for the surface of FeGa and FeNi. Thus, with FeGa on top or FeNi on top, the magnetic properties would be very different for various morphologies of the interface.

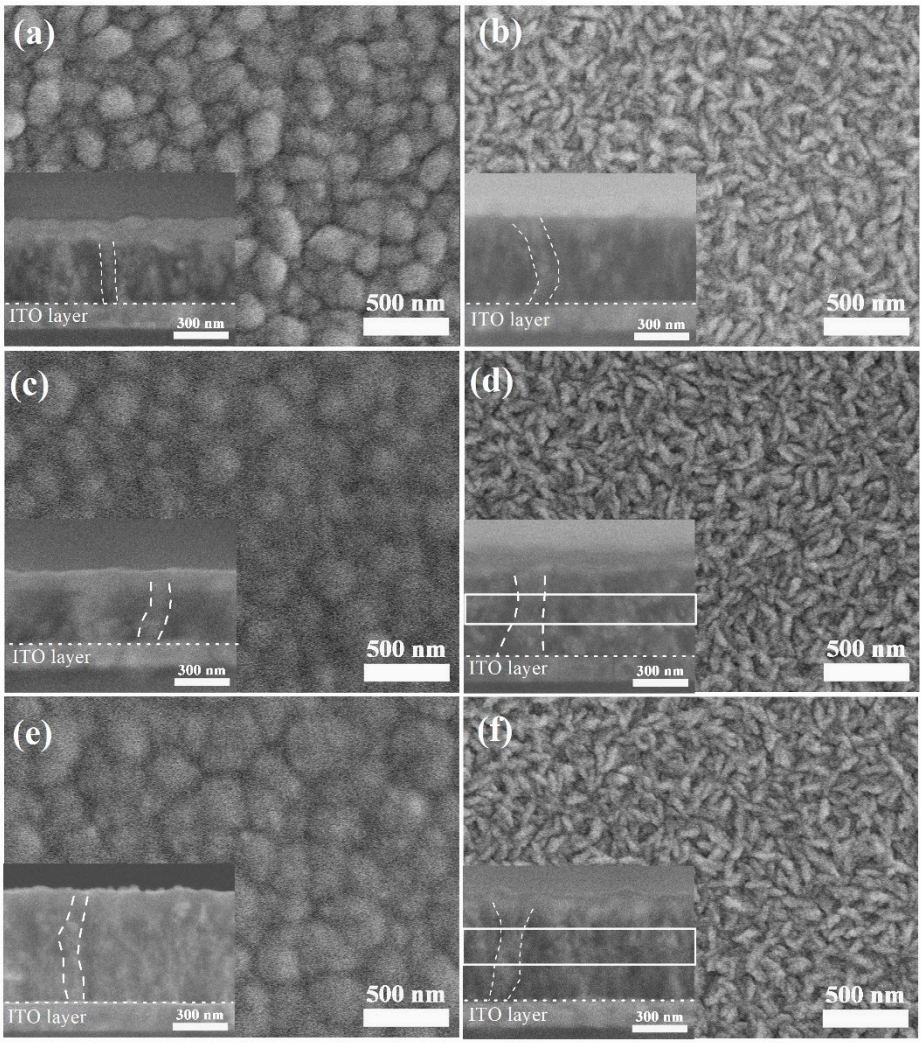

Figure 2. SEM image of SA1 (**a**), SA2 (**b**), SB1 (**c**), SB2 (**d**), SC1 (**e**), and SC2 (**f**). The insets show SEM cross-sectional images of the films.

3.2. Static Magnetic Properties of FeGa/FeNi (FeNi/FeGa) Films

The typical hysteresis loops of SA1, SA2, SB1, SB2, SC1, SC2, FeNi (500 s), and FeGa (500 s) are shown in Figure 3. The coercive field (H_c) and remanence magnetization (M_r) to the saturation magnetization (M_s) ratio (M_r/M_s) are shown in Table 2. One can see that H_c for FeGa on top is smaller than that of FeNi on top which means that with FeGa on top the samples show better soft magnetic properties. This may be the result of various interface coupling interactions for the inverse deposition order. From Table 2, the H_c increases with the ratio FeNi in the bilayer structure, but the M_r/M_s decreases. For single films, H_c of FeNi is larger than that of FeGa, while M_r/M_s is smaller than that of FeGa. When they are fabricated as bilayer structures, the proportion of FeNi and FeGa in the bilayer structure affects the H_c and M_r/M_s. We also investigate the in-plane angular dependence and all the samples show isotropic magnetism in-plane. In additional, for single FeNi and FeGa film, H_c is 50.4 and 36.4 Oe which is larger than that of the bilayer samples. This is because the interface coupling interaction between the two layers can reduce the energy required for the magnetization to flip in this bilayer structure [20]. The results are similar in the high magnetization of the soft phase and the high coercivity of the hard phase bilayer structures [21].

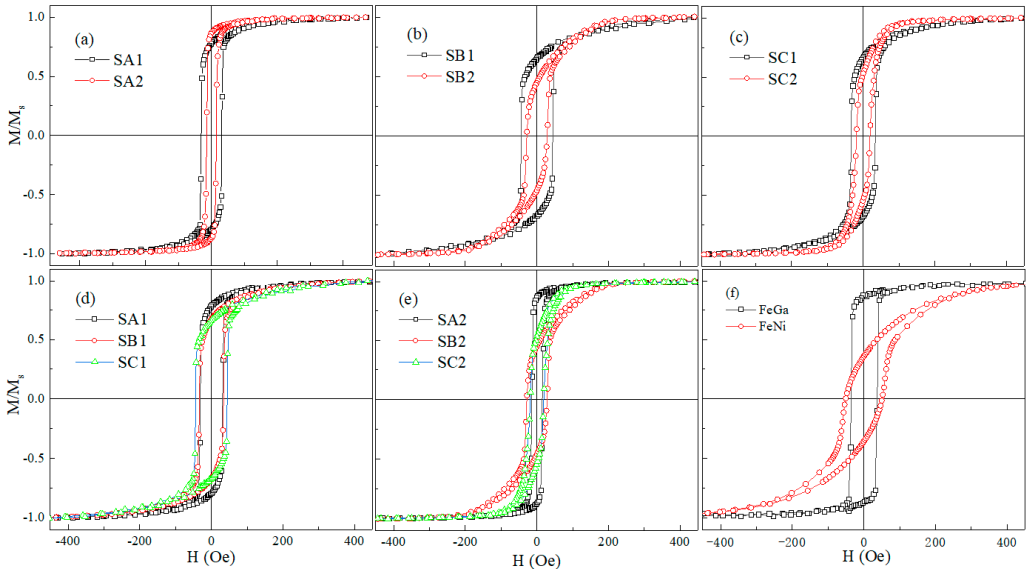

Figure 3. Hysteresis loops of SA1, SA2, SB1, SB2, SC1, SC2, FeNi (500 s), and FeGa (500 s). The comparison of loops for SA1 and SA2 (**a**), SB1 and SB2 (**b**), SC1 and SC2 (**c**). The loops of FeNi on top layer (**d**). The loops of FeGa on top layer (**e**). The loops of single FeNi and FeGa (**f**).

Table 2. H_c and M_r/M_s of SA1, SA2, SB1, SB2, SC1, SC2, FeNi (500 s), and FeGa (500 s).

Samples	SA1	SA2	SB1	SB2	SC1	SC2	FeNi	FeGa
H_c (Oe)	32.0	13.7	43.9	27.4	34.1	18.9	50.4	36.4
M_r/M_s	0.78	0.87	0.65	0.45	0.67	0.53	0.35	0.86

3.3. Dynamic Magnetic Properties of FeGa/FeNi (FeNi/FeGa) Films

The dynamics magnetism of FeNi/FeGa (FeGa/FeNi) bilayer structures has been studied by ferromagnetic resonance (FMR) which is one of the ideal techniques to study dynamics magnetism. The FMR as a function of the field is applied in the plane of the film as shown in Figure 4; one can see that the resonance peak moves to the high field with the increase of FeNi proportion for both samples of FeNi on top and FeGa on top. Meanwhile, for FeGa on top the resonance peak is higher than that of FeNi on top, which may be result of different coupling interactions between FeNi and FeGa layers. The resonance field of SA1, SB1, SC1, SA2, SB2, and SC2 is 26.1, 47.9, 60.5, 40.7, 62.9,

and 60.9 mT, respectively. The linewidth of SA1, SB1, SC1, SA2, SB2, and SC2 is 46.4, 35.8, 36.7, 54.9, 27.81, and 37.26 mT, respectively. These results are similar with the bilayer structure of FeGa/FeNi in another study [11]. Meanwhile, the spectra of FMR are almost symmetrical and the maximum peak strength indicates that the samples have better soft magnetic property [23,24]. We also measured the FMR with different angles in-plane which are almost in the same position with similar curves. This means that the samples show isotropic magnetism which responds to the VSM results.

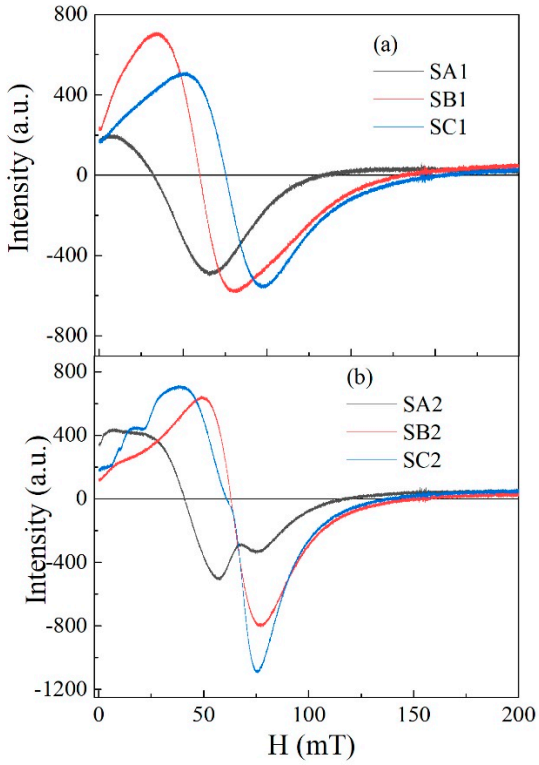

Figure 4. Ferromagnetic resonance (FMR) spectra of FeNi/FeGa (FeGa/FeNi) samples. (**a**) is the FMR image of SA1, SB1 and SC1, (**b**) is the FMR image of SA2, SB2 and SC2.

In order to quantitatively understand the dynamic properties of these bilayer structures, the experiment measured the frequency dependence of real (μ') and imaginary (μ'') permeability spectra, as displayed in Figure 5. We found that when FeNi is on top the permeability shows a weak peak for SA1, SB1, and SC1 (Figure 5a,c), while when FeGa is on top it shows a high permeability value which is enhanced several times for SA2, SB2, and SC2 (Figure 5b,d). Especially for SB2 and SC2 samples, a clear resonant phenomenon with resonant frequency band appears. For the single FeGa film (Figure 5a,c), the permeability is a similar value with FeNi on the top. Meanwhile, for single FeNi film, the permeability value is weaker than that of FeGa on top. Generally, the coupling interaction between the bilayer could affect the magnetic properties of the sample. From SEM images in Figure 2, the morphology is very different for the surface of FeGa and FeNi. The different deposition order could induce different interface coupling interactions and influence the magnetic properties of the bilayer structure for samples of FeNi on top and FeGa on top. To further understand the resonant behavior, the spectrum of SB2 and SC2 were fitted by Landau–Lifshitz–Gibert equations in Figure 6 [25],

$$\mu' = 1 + \chi_0 \frac{1 + \left(\alpha^2 - 1\right)\left(\frac{f}{f_r}\right)^2}{\left[1 - (1 + \alpha^2)\left(\frac{f}{f_r}\right)^2\right] + \left(2\alpha\frac{f}{f_r}\right)^2}. \quad (1)$$

$$\mu'' = \chi_0 \frac{\alpha\left(\frac{f}{f_r}\right)\left[1+\left(1+\alpha^2\right)\left(\frac{f}{f_r}\right)^2\right]}{\left[1-(1+\alpha^2)\left(\frac{f}{f_r}\right)^2\right]+\left(2\alpha\frac{f}{f_r}\right)^2}. \quad (2)$$

where f is frequency, f_r is resonance frequency, $\chi_0 = \mu_i - 1$ is the initial susceptibility, and α is the damping coefficient. From the fitting, the parameters for SB2 are the following: f_r, χ_0, and α are 0.66 GHz, 200, and 0.5, respectively. For SC2, f_r, χ_0, and α are 0.47 GHz, 245, and 0.36, respectively. Compared with FeGa film from a previous study [7], the permeability of ours shows higher intensity, although the resonance frequency is lower. We speculate this is because our sample shows isotropic magnetism. For FeGa/NiFe heterostructures deposited by sputtering, the resonance peak of μ' and μ'' is at about 1 GHz, which is a little higher than ours [11]. Compared with sputtering, the electrodeposition method can cause more defects and high roughness in films, which could induce different magnetic properties [26]. Moreover, the defects and roughness can induce a large damping coefficient.

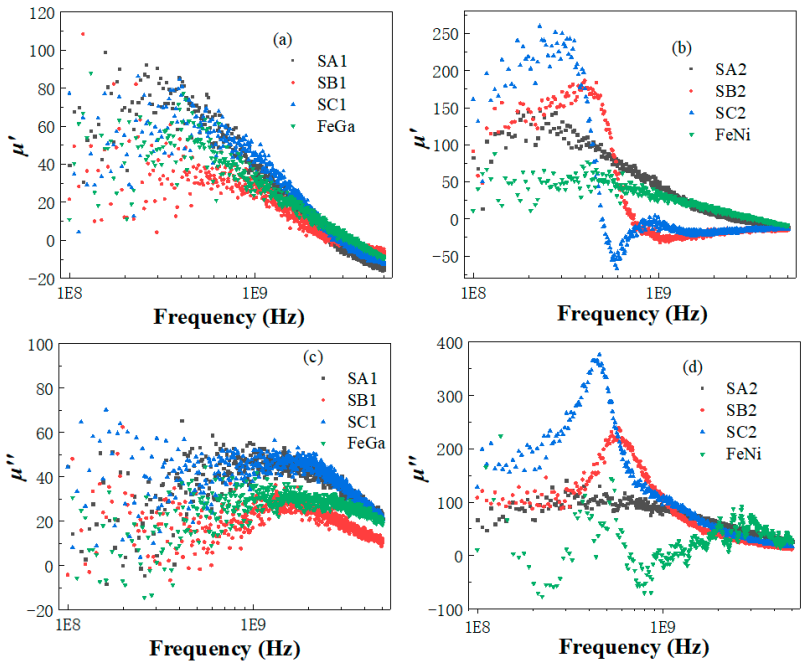

Figure 5. The real part and imaginary part of complex permeability of FeNi/FeGa (FeGa/FeNi) films, FeGa and FeNi. (**a**,**c**) show the real and imaginary part of SA1, SB1, SC1 and FeGa. (**b**,**d**) show the real and imaginary part of SA2, SB2, SC2 and FeN.

In general, hysteresis loss, domain-wall resonance, the eddy current effect, and natural resonance are responsible for permeability [27]. Firstly, the hysteresis loss could not be triggered for the weakly applied microwave field used. Secondly, the range of domain-wall resonance usually takes place at much lower than a gigahertz. Moreover, for our samples, the thickness is smaller than 1 μm, but the skin depth for the eddy current in the microwave frequency range is about 1 μm [28]. Then the eddy current can be precluded. Thus, the main magnetic loss mechanism could be natural resonance. Although the electrodeposition method is an easy way to reach large-scale production. Similar to the above, these results indicate that FeNi/FeGa bilayer structures have great potential for high-frequency applications. For the next step, we will try to induce anisotropy magnetism to enhance the resonance frequency in this bilayer structure.

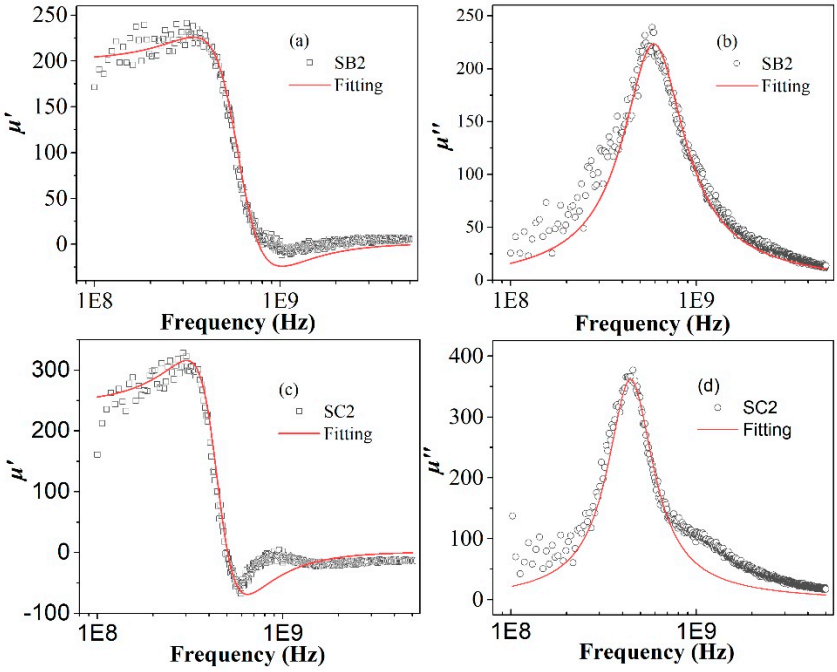

Figure 6. The fitting curves of the real permeability and imaginary permeability for SB2 and SC2. (**a**,**b**) show the fitting curves of SB2. (**c**,**d**) show the fitting curves of SC2.

4. Conclusions

FeGa/FeNi (FeNi/FeGa) bilayer structures with different thickness were deposited by the electrodeposition method on ITO substrates. The static and dynamic magnetic properties were investigated to tailor their magnetic softness, magnetization, ferromagnetic resonance, and permeability properties. The bilayer structures exhibit extremely various characters with different deposition order which attributes to the coupling interaction in the interface. With FeGa or FeNi on the top layer, the surface shows a different morphology and the bilayer structure, H_c is lower than FeNi on the top. Meanwhile, an increase in the proportion of FeNi or thickness in the bilayer structure would affect the H_c and M_r/M_s. Moreover, FeGa on top shows improved permeability and a clear resonant phenomenon of the magnetization. All the results imply that this structure may be a suitable candidate for high-frequency application.

Author Contributions: Conceptualization, Z.W. and F.W.; methodology, Z.W. and C.X.; investigation, Z.W. and C.X.; data curation, Z.W. and Z.H.; writing—original draft preparation, Z.W.; writing—review and editing, Z.H. and D.C.; project administration, Z.W. All authors have read and agreed to the published version of the manuscript.

Funding: This research was funded by the National Natural Science Foundation of China (No. 211012180393), the Fundamental Research Funds for the Central Universities (No. 300102129102, 300102128301), and the China Postdoctoral Science Foundation (No. 2017M3123).

Acknowledgments: The authors also gratefully acknowledge financial support from China Scholarship Council. We also thank the experimental environment help of Prof Tai Min from Xi'an Jiaotong University.

Conflicts of Interest: The authors declare no conflicts of interest.

References

1. Alvarez-Quiceno, J.C.; Cabrera-Baez, M.; Ribeiro, R.A.; Ávila, M.A.; Dalpian, G.M.; Osorio-Guillén, J.M. Emergence of competing magnetic interactions induced by Ge doping in the semiconductor $FeGa_3$. *Phys. Rev. B* **2016**, *94*, 014432. [CrossRef]
2. Fin, S.; Tomasello, R.; Bisero, D.; Marangolo, M.; Sacchi, M.; Popescu, H.; Eddrief, M.; Hepburn, C.; Finocchio, G.; Carpentieri, M.; et al. In-plane rotation of magnetic stripe domains in Fe_{1-x} Ga_x thin films. *Phys. Rev. B* **2015**, *92*, 224411. [CrossRef]

3. Clark, A.E.; Restorff, J.B.; Wun-Fogle, M.; Lograsso, T.A.; Schlagel, D.L. Magnetostrictive properties of body-centered cubic Fe-Ga and Fe-Ga-Al alloys. *IEEE Trans. Magn.* **2000**, *36*, 3238–3240. [CrossRef]
4. Atulasimha, J.; Flatau, A.B. A review of magnetostrictive iron–gallium alloys. *Smart Mater. Struct* **2011**, *20*, 043001. [CrossRef]
5. Kuanr, B.K.; Camley, R.E.; Celinski, Z.; McClure, A.; Idzerda, Y. Single crystal Fe1—xGax thin films for monolithic microwave devices. *J. Appl. Phys.* **2014**, *115*, 17C112. [CrossRef]
6. Osaka, T.; Takai, M.; Hayashi, K.; Ohashi, K.; Saito, M.; Yamada, K. A soft magnetic CoNiFe film with high saturation magnetic flux density and low coercivity. *Nature* **1998**, *392*, 796–798. [CrossRef]
7. Yu, Y.; Zhan, Q.; Wei, J.; Wang, J.; Dai, G.; Zuo, Z.; Zhang, X.; Liu, Y.; Yang, H.; Zhang, Y.; et al. Static and high frequency magnetic properties of FeGa thin films deposited on convex flexible substrates. *Appl. Phys. Lett.* **2015**, *106*, 162405. [CrossRef]
8. Ge, J.; Sun, L.; Zhang, F.R.; Zhang, Y.; Shi, L.A.; Zhao, H.Y.; Zhu, H.W.; Jiang, H.L.; Yu, S.H. A stretchable electronic fabric artificial skin with pressure-, lateral strain-, and flexion-sensitive properties. *Adv. Mater.* **2016**, *28*, 722–728. [CrossRef] [PubMed]
9. Zhang, X.; Zhan, Q.; Dai, G.; Liu, Y.; Zuo, Z.; Yang, H.; Chen, B.; Li, R.W. Effect of buffer layer and external stress on magnetic properties of flexible FeGa films. *J. Appl. Phys.* **2013**, *113*, 17A901. [CrossRef]
10. Cao, D.; Wang, Z.; Pan, L.; Feng, H.; Cheng, X.; Zhu, Z.; Wang, J.; Liu, Q.; Han, G. Controllable magnetic and magnetostrictive properties of FeGa films electrodeposited on curvature substrates. *Appl. Phys. A* **2016**, *122*, 938. [CrossRef]
11. Rementer, C.R.; Fitzell, K.; Xu, Q.; Nordeen, P.; Carman, G.P.; Wang, Y.E.; Chang, J.P. Tuning static and dynamic properties of FeGa/NiFe heterostructures. *Appl. Phys. Lett.* **2017**, *110*, 242403. [CrossRef]
12. Pérez-Landazábal, J.I.; Recarte, V.; Sánchez-Alarcos, V.; Rodríguez-Velamazán, J.A.; Jiménez-Ruiz, M.; Link, P.; Cesari, E.; Chumlyakov, Y.I. Lattice dynamics and external magnetic-field effects in Ni-Fe-Ga alloys. *Phys. Rev. B* **2009**, *80*, 144301. [CrossRef]
13. Zhang, Y.; Gan, T.; Wang, T.; Wang, F.; Shi, W. Giant magnetoimpedance effect in $Fe_{75.5}Cu_1Nb_3Si_{13.5}B_7$ ribbon/FeGa film composite. *J. Magn. Magn. Mater.* **2016**, *417*, 37–41. [CrossRef]
14. Lupu, N.; Chiriac, H.; Pascariu, P. Electrochemical deposition of FeGa/Ni Fe magnetic multilayered films and nanowire arrays. *J. Appl. Phys.* **2008**, *103*, 07B511. [CrossRef]
15. Dai, G.; Xing, X.; Shen, Y.; Deng, X. Stress-controlled dynamic susceptibility in FeGa stripes. *J. Appl. Phys.* **2018**, *123*, 243902. [CrossRef]
16. Endo, Y.; Sakai, T.; Miyazaki, T.; Shimada, Y. Effect of Film Thickness on the High Frequency Magnetic Properties of Polycrystalline Fe–Ga Films. *IEEE Trans. Magn.* **2017**, *53*, 1–5. [CrossRef]
17. Tran, T.Q.; Lee, J.K.Y.; Chinnappan, A.; Jayathilaka, W.A.D.M.; Ji, D.; Kumar, V.V.; Ramakrishna, S. Strong, lightweight, and highly conductive CNT/Au/Cu wires from sputtering and electroplating methods. *J. Mater Sci. Technol.* **2020**, *40*, 99–106. [CrossRef]
18. Tran, T.Q.; Lee, J.K.Y.; Chinnappan, A.; Loc, N.H.; Tran, L.T.; Ji, D.; Jayathilaka, W.A.D.M.; Kumar, V.V.; Ramakrishna, S. High-performance carbon fiber/gold/copper composite wires for lightweight electrical cables. *J. Mater Sci. Technol.* **2020**, *42*, 46–53. [CrossRef]
19. Zhang, X.; Zhan, Q.; Dai, G.; Liu, Y.; Zuo, Z.; Yang, H.; Chen, B.; Li, R.W. Effect of mechanical strain on magnetic properties of flexible exchange biased FeGa/IrMn heterostructures. *Appl. Phys. Lett.* **2013**, *102*, 022412. [CrossRef]
20. Jiang, J.S.; Bader, S.D. Magnetic reversal in thin film exchange-spring magnets. *Scr. Mater.* **2002**, *47*, 563–568. [CrossRef]
21. Fullerton, E.E.; Jiang, J.S.; Bader, S.D. Hard/soft magnetic heterostructures: Model exchange-spring magnets. *J. Magn. Magn. Mater* **1999**, *200*, 392–404. [CrossRef]
22. Zhang, Y.; Huang, C.; Duan, Z.; Shi, W. Tuning static and dynamic magnetic properties of FeGa/Mn film. *J. Magn. Magn. Mater.* **2019**, *477*, 4–8. [CrossRef]
23. Sun, K.; Pu, Z.; Yang, Y.; Chen, L.; Yu, Z.; Wu, C.; Jiang, X.; Lan, Z. Rietveld refinement, microstructure and ferromagnetic resonance linewidth of iron-deficiency NiCuZn ferrites. *J. Alloys Compd.* **2016**, *681*, 139–145. [CrossRef]
24. Wang, Z.; Feng, E.; Zhang, Y.; Liu, Q.; Wang, J. Optimum electrodeposition conditions of FeCoZr films with in-plane uniaxial anisotropy for high frequency application. *Mater. Chem. Phys.* **2012**, *137*, 499–502. [CrossRef]

25. Wei, J.; Wang, J.; Liu, Q.; Li, X.; Cao, D.; Sun, X. An induction method to calculate the complex permeability of soft magnetic films without a reference sample. *Rev. Sci. Instrum.* **2014**, *85*, 054705. [CrossRef]
26. Raveendran, N.L.; Pandian, R.; Murugesan, S.; Asokan, K.; Kumar, R.R. Phase evolution and magnetic properties of DC sputtered Fe-Ga (Galfenol) thin films with growth temperatures. *J. Alloys Compd.* **2017**, *704*, 420–424. [CrossRef]
27. Ma, J.; Li, J.; Ni, X.; Zhang, X.; Huang, J. Microwave resonance in Fe/SiO_2 nanocomposite. *Appl. Phys. Lett.* **2009**, *95*, 102505.ss. [CrossRef]
28. Yan, L.; Wang, J.; Han, X.; Ren, Y.; Liu, Q.; Li, F. Enhanced microwave absorption of Fe nanoflakes after coating with SiO_2 nanoshell. *Nanotechnology* **2010**, *21*, 095708. [CrossRef]